JOURNAL OF KUFA–PHYSICS
journal.uokufa.edu.iq/index.php/jkp/index | ISSN: 2077–5830

Preparation of ($HgBa_2Ca_2Cu_{2.85}La_{0.15}O_{8+\delta}$) superconducting compound and Study the impact of partial substitution of mercury with (In_2O_3) on the structural characteristics

*** Ekhlas Hassan**[1] **Haider MJ. Haider**[2]

[1]*Material Department, Faculty of Engineering, University of Kufa, Najaf, IRAQ*
[2]*Physics Department, College of Education for Girls, University of Kufa, Najaf, IRAQ .*

[*]Corresponding Author E-mail: eklaseh.alkhazraji@uokufa.edu.iq

ARTICLE INF

Article history:
Received: 30 DEC, 2022
Revised: 03 FEB, 2023
Accepted: 05 FEB, 2023
Available Online: 03 JUN, 2023

Keywords:

Partial substitution
the (SSR) method
(XRD) analysis
degree of crystallinity
crystallite size and strain

ABSTRACT

In the current work, we focused on the impact of Indium oxide partial substitution at the (Hg) site on the structural characteristics of the ($HgBa_2Ca_2Cu_{2.85}La_{0.15}O_{8+\delta}$) compound with (0,0.05,0.1,0.15,0.2 and 0.25). Samples were prepared by the (SSR) method. The combined powder was crushed with a pressure of 7 tons per square centimeter to create a disc with a thickness of (0.2 cm) and a diameter of (1.5 cm). The samples sintered for 24 hours at a rate that was changed from ambient temperature to 820 °C. For the samples which were doped with (In=0.05) in comparison to other samples, the highest value of the c-axis lattice parameter and a pseudo-tetragonal structure were discovered using (XRD) analysis. It was discovered that altering the In concentrations in all of the results of our sample changes the volume fraction V_{Ph}(1223), mass density d_m, and c/a. It was also determined that the change in lattice parameters, degree of crystallinity, crystal size, and strain (in different ways) resulted from a change in the indium oxide concentrations for all samples.

DOI: https://doi.org/10.31257/2018/JKP/2023/v15.i01.10917

تحضير المركب ($HgBa_2Ca_2Cu_{2.85}La_{0.15}O_{8+\delta}$) ودراسة تأثير الإستبدال الجزئي للزئبق ب(In_2O_3) على الخواص التركيبية

اخلاص حسن[1] **حيدر محمد جواد حيدر**[2]

[1] قسم هندسة المواد، كلية الهندسة، جامعة الكوفة، النجف، العراق.
[2] قسم الفيزياء، كلية التربية للبنات،جامعة الكوفة، النجف، العراق

الـــخُـــلاصـــة

في العمل الحالي ،إجرينا دراسة حول تأثير الاستبدال الجزئي لأكسيد الإنديوم في موقع *(Hg)*على الخصائص التركيبية للمركب *($HgBa_2Ca_2Cu_{2.85}La_{0.15}O_{8+\delta}$)*بنسب إستبدال (٠,٠.٠٥,٠.١,٠.١٥,٠.٢,٠.٢٥). تم تحضير العينات بطريقة تفاعل الحالة الصلبة *(SSR)*

الكلمات المفتاحية:

الاستبدال الجزئي
بطريقة تفاعل الحالة الصلبة *(SSR)*
تحليل *(XRD)*
درجة التبلور
حجم البلورة، والانفعال

.تم كبس مسحوق المركب بضغط ٧ طن لكل سنتيمتر مربع لتكوين قرص بسمك (٠.٢ سم) وقطر (١.٥ سم). لبدت العينات لمدة ٢٤ ساعة بمعدل تغير من درجة الحرارة الغرفة إلى ٨٢٠ درجة مئوية. بالنسبة للعينات التي تحتوي نسبة الإستبدال(*In =0.05*) مقارنة بالعينات الأخرى ، تم اكتشاف أعلى قيمة لمعامل شبيكة المحور *c* وتركيب*tetragonal*باستخدام تحليل (*XRD*). تم اكتشاف أن تغيير التراكيز في جميع نتائج العينة يغير الكسر الحجمي *V_{Ph}(1223)* وكثافة الكتلية *dm* و *c/ a*. تم استخدام تحليل *XRD* لتحديد معاملات الشبيكة ، ودرجة التبلور وحجم البلرة ، والانفعال (بطرق مختلفة) حيث إنها تتغير مع تغير تراكيز أكسيد الإنديوم لجميع العينات.

1. INTRODUCTION

It has been discovered that there is a distinction between substances and chemical elements when it comes to electrical resistance or conductivity. Since the early of 1960s, superconducting materials have demonstrated distinctive and inherent properties, making them crucial for electronic device applications that call for cooling at extremely low temperatures[1-3]. Because of their high transition temperatures, mercury-based superconducting capsules like $HgBa_2CuO_{4+\delta}$(T_c=940k), $HgBa_2CaCu_2O_{6+\delta}$(T_c=127^0k), and $HgBa_2Ca_2Cu_3O_{8+\delta}$($T_c$=$134^0$k) are considered to be among the high-temperature superconducting materials [4]. By processing it in a furnace with high pressure, the critical transition temperature has risen to 160 K[5].

Extensive research on superconductivity has been performed with encouraging outcomes since the discovery of the first high-temperature superconductors based on mercury (Hg-1201) material with a high Tc. Many of the major problems with superconductivity remain involve superconducting materials, despite the field's enormous achievements. The difficulty of shaping these materials into wires or circuits such that they may transport high currents that are not permitted in typical conductors is one of these difficulties and has been a key problem ever since superconductivity was discovered[6-8]. One of the systems in the HBCCO family of superconducting mercury compounds is this one, the high-critical temperature superconducting material is produced by a Mercury oxide airplane [9].

According to several studies, favorable alternatives boost the phase development and superconducting characteristics of (Hg-1223). The partial substitution of some higher valence elements, such as Pb, Y, or Re, or other elements, might enhance the critical current density and phase development of Mercury -1223[5].

They have not used the Hg-Base family as frequently as other HTSC materials. This is because HTSC phases containing mercury are extremely difficult to synthesize and extremely susceptible to contamination by moisture and carbon dioxide. Samples of Mercury-Base are known to degrade fast after production. To increase the stability of the HTSC Mercury-Base stage, a lot of work has been done recently[3].

In the current study, (SSR) method was used to create polycrystalline compounds of ($Hg_{1-x}In_xBa_2Ca_2Cu_{2.85}La_{0.15}O_{8+\delta}$) where (x=0, 0.05, 0.1, 0.15, 0.20, 0.25). We will examine the structural characteristics of compounds and investigate the impact of partial Indium substitution on crystallinity degree, crystallite size, and strain (using multiple methods).

2. EXPERIMENTAL DETAILS

Using the (SSR) method, the superconducting compound ($Hg_{1-x}In_xBa_2Ca_2Cu_{2.85}La_{0.15}O_{8+\delta}$) with (x=0, 0.05,

0.1, 0.15, 0.20, 0.25), was prepared by using suitable weights of powders of (HgO, BaO, CaO, CuO, La_2O_3, In_2O_3) (with a purity of more than 99.9%). With sensitivity order (10^{-4}) g, a sensitive balance was used to estimate the reactants. To homogenize the reactants, isopropanol ($C_2H_3O_5$) was added and the reactants were mixed in a gate mortar for two hours to obtain fineness and optimal homogeneity of the powders, then the resulting powders were dried at a temperature of 200 ^oC for a period of (1hr) in a drying oven. The samples were compressed into discs with a thickness of (0.2cm) and a diameter of (1.5 cm) using a hydraulic press under pressure (7 tons/cm^2) for one minute. To produce a coherent material and to assure the process, the samples were sintered inside a sintering furnace for 24 hours at a temperature of 820 degrees Celsius. The temperature was progressively raised (i.e. at the rate of 10 ^oC/min). The samples were gradually cooled within the furnace at the same heating rate after optimal atoms diffusion. To determine the samples' structural characteristics, the samples were examined at within the diffraction angle range (10-80). The constants (a,

b, and c) were determined theoretically using Miller indices and d-values of the observed XRD pattern reflections. Additionally, the cell unit density was determined, and the percentages of the phases created in the samples were calculated using the equation below [10, 11]:

$$(V_{Ph})\% = \frac{\sum I_0}{\sum I_1 + \sum I_2 + \sum I_{other(peaks)}} \times 100\% \dots\dots\dots 1$$

and the concentrations of hole per Cu ion(P) was calculated by means of [12]:

$$P = (0.16) - [(1 - T_C/T_{C\,max})/(82.6)]^{1/2} \dots\dots 2$$

Investigation of the impact of partial substitution of concentrations on the degree of crystallinity, and crystallite size, strain was conducted using various techniques.

3. RESULTS AND DISCUSSION

The produced samples of ($Hg_{1-x}In_xBa_2Ca_2Cu_{2.85}La_{0.15}O_{8+\delta}$) were seen to have various Indium concentrations(x=0, 0.05, 0.1, 0.15, 0.20, 0.25) that were given a general structural analysis using the (XRD) method. All of the samples were polycrystalline and correlate to tetragonal, according to the (XRD) data gathered from a variety of samples. In Fig.1, the representative (XRD) pattern is displayed. The spectra revealed that all samples were composed mostly of some impurity phases in addition to the low -Tc phase(1212) and the high-Tc phase (1223). The arranging defects throughout the c-axis may be the cause of the emergence of more than two phases [13]. According to a comparison of the XRD patterns', the relative intensities for samples with ln=0.05, 0.15, 0.2, and 0.25 with the same reflections' relative intensity in the sample with ln=0.0, all samples have reflection intensities of the High-Tc phase reflections (peaks H) and Low-Tc phase reflections (peaks L), with the (peaks H) changing and the (peaks L) is changing with changing ln.

Table 1 shows the lattice constants (a, b, and c), mass density d_m, and (V phase) which were found through the results of (XRD).

The conduction channel in Hg-base is holes in the Cu-O_2 layers, which are strengthened by the Hg-O layer, as a result of the replacement of ln for Hg owing to the different ionic radii. Hg-1223's charge transfer from the Hg layer to the Cu layer is adjusted by the c-axis' deformation[13].

Crystallite size, strain, and degree of crystallinity are calculated using XRD analysis. Different techniques were used to determine the crystal size, including the Halder-Wagner Langford method, the modified Scherrer

method, the Williamson-Hall method, and the Size-strain plot approach.

Table 1: Demonstrates the generated samples' phase ratios, lattice coefficients, (c/a), and density.

X	a=b (A^0)	c (A^0)	c/a	V ($(A^0)^3$)	Dm (gm/cm^3)	Vph (H)	Vph (L)	Tc (K)	P
0	3.892	15.865	4.076	240.365	6.122	77.3	27.7	120.4	0.1266
0.05	3.841	16.065	4.182	237.040	6.208	80	20	132.6	0.16
0.1	3.895	15.863	4.072	240.688	6.114	78.3	21.7	121.6	0.1283
0.15	3.895	15.874	4.074	240.900	6.109	72.7	27.3	118.8	0.1245
0.2	3.836	15.865	4.135	233.546	6.301	77.3	22.7	120.5	0.1267
0.25	3.889	15.589	4.008	235.818	6.240	72.7	27.3	116.2	0.1213

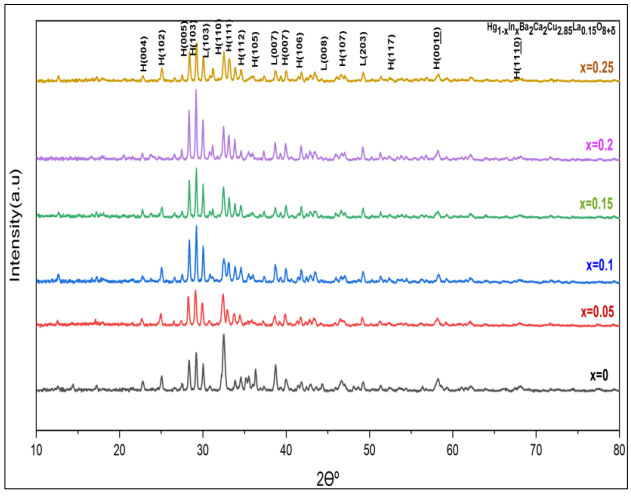

Figure 1: X-ray diffraction for ($Hg_{1-x}In_xBa_2Ca_2Cu_{2.85}La_{0.15}O_{8+\delta}$) bulk polycrystalline samples where (x=0, 0.05, 0.1, 0.15, 0.20, 0.25).

Table 2: Crystallite size and degree of crystallinity of ($Hg_{1-x}In_xBa_2Ca_2Cu_{2.85}La_{0.15}O_{8+\delta}$) compound using different Methods.

X	Cryestilanity (%)	crystallite size (D) (nm)				
		Scherrer method	modified Scherrer method	Williamson-Hall method	Size-strain plot method	Halder-Wagner Langford method
0	54.39	30.915	37.234	62.739	30.743	30.788
0.05	63.51	28.337	33.882	45.460	27.240	30.257
0.1	60.84	33.175	35.906	35.643	37.272	41.356
0.15	56.42	37.942	45.178	83.026	23.264	25.853
0.2	58.93	28.981	26.788	21.904	19.045	21.168
0.25	55.76	32.624	35.648	63.895	34.320	38.153

Table 3: Strain of ($Hg_{1-x}In_xBa_2Ca_2Cu_{2.85}La_{0.15}O_{8+\delta}$) compound using different Methods.

X	strain(ε)		
	Williamson-Hall method	Size-strain plot method	Halder-Wagner Langford method
0	0.00234	0.001016883	0.00128688
0.05	1.39E-03	0.000139781	0.000907313
0.1	3.99E-04	0.000545328	0.003539712
0.15	2.10E-03	0.001302404	0.008453875
0.2	5.16E-04	0.001378669	0.008948899
0.25	2.39E-03	7.09132E-05	0.000460296

3.1 Scherrer Method

Eq.2 refers to The Scherrer equation, which is mostly based on data from X-ray diffraction, which is a formula that links the average crystal size in materials to a peak expansion in the diffraction pattern. The scientist (Paul Shearer) gave it its name. The average crystallite size (D) in the crystal's vertical direction was calculated using the following Scherrer formula [14, 15].

$$D = \frac{K\lambda}{\beta_{hkl} COS\theta} \dots\dots\dots 2$$

where K=0.9 (constant), The wavelength of an X-ray is (λ =0.15406 nm), and β_{hkl} = highest peak intensity at full width in Radian (FWHM). Utilizing the Origin program, the crystallite size may be calculated. Fig.2 shows a graph of (cosθ) as a function of ($1/ß_{hkl}$) for ($Hg_{0.95}In_{0.05}Ba_2Ca_2Cu_{2.85}La_{0.15}O_{8+\delta}$) bulk polycrystalline using the Origin software. The average crystallite size can be calculated from the Eq.2 which was found as (30.9154064) nm.

Similarly, the crystallite size of ($Hg_{1-x}In_xBa_2Ca_2Cu_{2.85}La_{0.15}O_{8+\delta}$) was calculated when (X =0,0.1,0.15,0.2 and 0.25), and their values are presented in the Table 2.

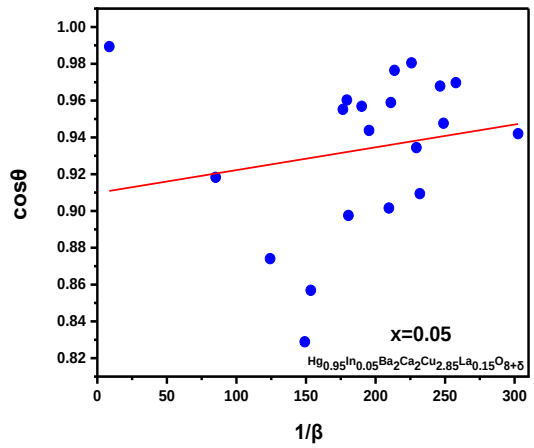

Figure 2: Graph of cosθ as a function of 1/ßhkl for ($Hg_{0.95}In_{0.05}Ba_2Ca_2Cu_{2.85}La_{0.15}O_{8+\delta}$) bulk polycrystalline presented to Scherrer crystallite size.

The crystal volume was also calculated using the Modified Scherrer equation, which is calculated by taking (Ln) to both sides of Eq.3, so we get the following equation[16]:

$$Ln(\beta) = Ln\left(\frac{1}{cos\theta}\right) + Ln\left(\frac{K\lambda}{D}\right) \dots\dots\dots 3$$

This equation represents a straight-line equation between $Ln(\beta)$ on a Y-axis and $Ln\left(\frac{1}{cos\theta}\right)$ on an X-axis using the Origin software, then

$$\text{Intercept} = Ln\left(\frac{K\lambda}{D}\right) \rightarrow D = \frac{K\lambda}{e^{(\text{Intercept}}} \dots . 4$$

From Fig. 3 and Eq.4 the crystallite size(D) can be calculated, where the corresponding values are shown in Table 2.

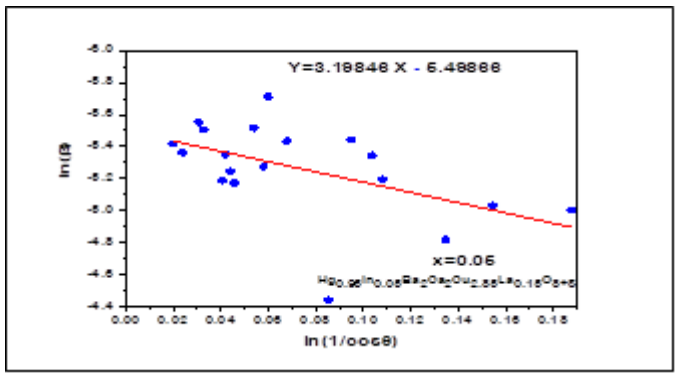

Figure 3: Graph of $Ln(\beta)$ as a function of $Ln\left(\frac{1}{cos\theta}\right)$for($Hg_{0.95}In_{0.05}Ba_2Ca_2Cu_{2.85}La_{0.15}O_{8+\delta}$) bulk polycrystalline presented to The Modified Scherrer crystallite size.

3.2 Williamson-Hall (W-H) method

This is a way to determine the crystallite size and strain of crystals. The size causes the physical line broadening of the XRD peak.

Peak widening is only taken into account by the (W-H) system as a function of a diffraction angle (2θ). This is thought to have been a combination of size- and strain-induced widening.

Consequently, the total broadening resulting from size and strain at a certain peak with the hkl value may be represented as follows:

$$\beta_{hkl} = (\beta_{hkl})size + (\beta_{hkl})strain \dots\dots\dots 5$$

The peak broadening caused by strain may be demonstarted as

$$(\beta_{hkl})strain = 4\,\varepsilon\, sin\theta \dots\dots\dots 6$$

Where ε (slop) represents the strain [15, 17, 18].

$$\beta_{hkl} = \frac{K\lambda}{D\, cos\theta} + 4\,\varepsilon\, tan\theta \dots\dots\dots 7$$

When rearranging Eq.8 we get:

$$\beta_{hkl}\, cos\theta = \frac{K\lambda}{D} + 4\,\varepsilon\, sin\theta \dots\dots\dots 8$$

Which represents straight line equation between$\beta_{hkl}\, cos\theta$ on a Y-axis and $4\, sin\theta$ on an X-axis using the Origin software, then

$$\text{Intercept} = \left(\frac{K\lambda}{D}\right) \quad \rightarrow D = \frac{K\lambda}{\text{Intercept}} \ldots\ldots 9$$

From Fig.4 and Eq.9 can be calculated crystallite size(D), that values are shown in Table2.

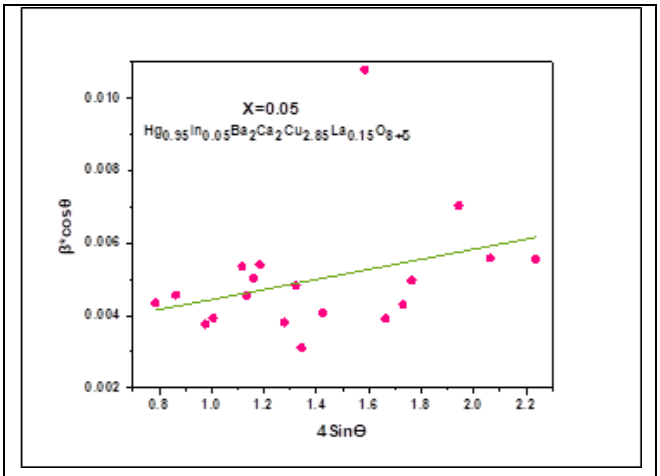

Figure 4: Graph of $\beta_{hkl}\ cos\theta$ as a function of $4\ sin\theta$ for ($Hg_{0.95}In_{0.05}Ba_2Ca_2Cu_{2.85}La_{0.15}O_{8+\delta}$) bulk polycrystalline presented to Williamson-Hall method.

3.3 The Size-strain plot (SSP) method

The (SSP) approach provides better isotropic expansion performance because it focuses on low angle reflections, where the resolution is higher than at higher angles. This is because the peaks in the XRD data at low angles usually overlap due to overlapping phases. Consequently, The (SSP) method, which examines peak profiles, ignores the lattice microstructures and only considers how crystalline size affects XRD peak broadening.

The following formula is used to do SSP measurement[14, 19, 20]:

$$[d_{hkl} * \beta_{hkl} * cos\theta]^2 = \frac{K\lambda}{D} * \left[{d_{hkl}}^2 * \beta_{hkl} * cos\theta\right] + \frac{\varepsilon^2}{4} \ldots\ldots 10$$

Which represents straight line equation between $[d_{hkl} * \beta_{hkl} * cos\theta]^2$ on a Y-axis and $\left[{d_{hkl}}^2 * \beta_{hkl} * cos\theta\right]$ on an X-axis using the Origin software, then

$$\text{Intercept} = \frac{\varepsilon^2}{4} \quad \rightarrow \varepsilon = \sqrt{4 * \text{Intercept}} \ldots\ldots 11$$

$$\text{slope} = \left(\frac{K\lambda}{D}\right) \quad \rightarrow D = \frac{K\lambda}{\text{slope}} \ldots\ldots 12$$

From Fig.5 and Eq.12 crystalline size(D) can be calculated, where it values are presented in Table 2.

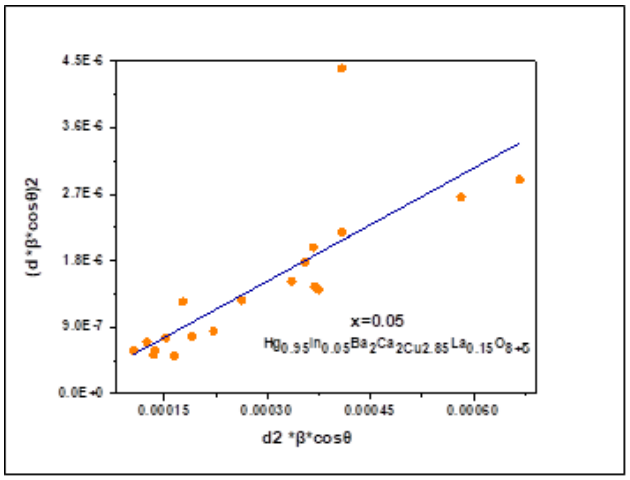

Figure 5: Graph of $[d_{hkl} * \beta_{hkl} * cos\theta]^2$ as a function of $\left[{d_{hkl}}^2 * \beta_{hkl} * cos\theta\right]$ for ($Hg_{0.95}In_{0.05}Ba_2Ca_2Cu_{2.85}La_{0.15}O_{8+\delta}$) bulk polycrystalline presented to Size-strain plot (SSP).

3.4 Halder-Wagner Langford method

The advantage of using this strategy is that peaks in the low-frequency range are focused on, the deviation peaks overlapping with the much lower, mid-angle regions, Peak broadening is considered to be a symmetrical Voigt function in the (HW) method.

The connection between crystallite size and lattice strain is now provided by the Halder-Wagner process and is as follows[20-22]:

$$\left(\frac{\beta_{hkl}}{d_{hkl}}\right)^2 = \frac{1}{D}\left(\frac{\beta_{hkl}}{{d_{hkl}}^2}\right) + \left(\frac{\varepsilon}{2}\right)^2 \ldots\ldots 13$$

The aforementioned equation is a straight-line equation, hence we will now create a graph of$\left(\frac{\beta_{hkl}}{d_{hkl}^2}\right)$vs. $\left(\frac{\beta_{hkl}}{d_{hkl}}\right)^2$, as shown in Fig.6, where $\left(\frac{\beta_{hkl}}{d_{hkl}^2}\right)$ on the X- axis and$\left(\frac{\beta_{hkl}}{d_{hkl}}\right)^2$ on the Y-axis. This straight line's slope provides the value of (1/crystallite size) among them, we find the (D) shown in Table 2 and the Intercept represent $\left(\frac{\varepsilon}{2}\right)^2$, From this, we can find the strain (ε)which is shown in Table 3.

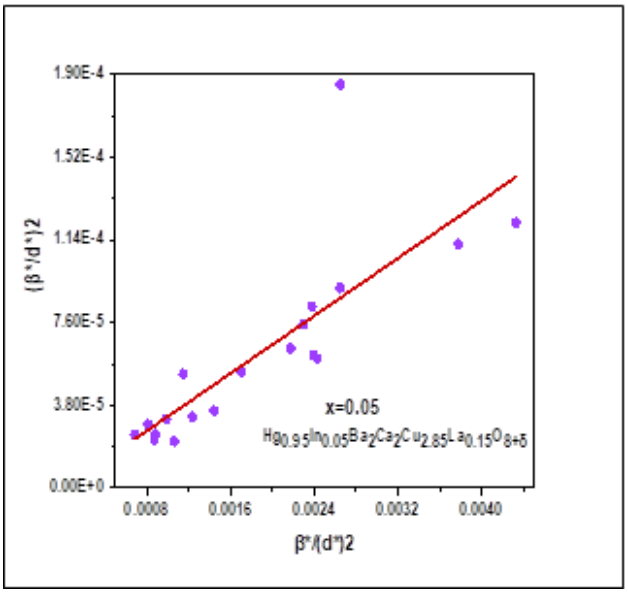

Figure 6: Graph of $\left(\frac{\beta_{hkl}}{d_{hkl}^2}\right)$ a function of $\left(\frac{\beta_{hkl}}{d_{hkl}}\right)^2$ for ($Hg_{0.95}In_{0.05}Ba_2Ca_2Cu_{2.85}La_{0.15}O_{8+\delta}$) bulk polycrystalline presented to Halder-Wagner Langford method.

3.5 The degree of Crystallinity

Typically, crystallinity is expressed as a percentage of the volume of the crystalline substance. However, even among perfectly crystalline materials, the level of structural perfection can vary. The following equation may be used to calculate the crystallinity using X-ray crystallography[14, 15]:

$$\textbf{Crystallinity} = \frac{\textbf{Area of crystalline peaks}}{\textbf{Area of all peaks(crystalline + Amorphus)}} \times 100\% \ldots\ldots\ldots 14$$

The findings that shown in Table 2 were obtained using the aforementioned equation. An illustration of the link between crystallinity levels and indium concentration is shown in Fig7. It should be noticed that when the indium concentration increased, the crystallization values changed.

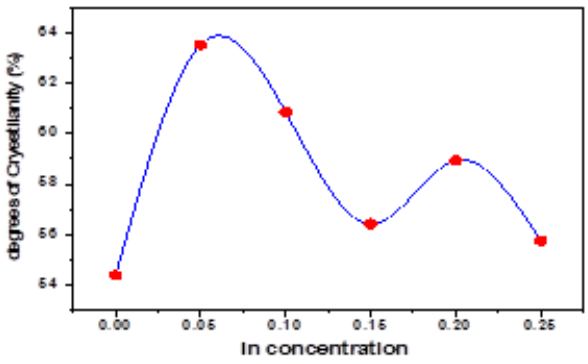

Figure 7: Degree of Crystallinity as a function of In concentration for ($Hg_{1-x}In_xBa_2Ca_2Cu_{2.85}La_{0.15}O_{8+\delta}$) bulk polycrystalline samples.

4. Conclusion

We have investigated the impact of the synchronic substitution at the Hg site in the HgO layer, which lacks oxygen of ($Hg_{1-x}In_xBa_2Ca_2Cu_{2.85}La_{0.15}O_{8+\delta}$) cuprate superconductor which has been prepared under optimum conditions. In comparison to samples without any In content, (XRD) examination revealed a pseudo-tetragonal structure with an increase in the c-axis lattice constant. As-grown samples' transition temperatures are discovered to be sensitive to In concentrations.

where the optimal value (Tc=132.6 k) occurs when focus (x = 0.05) coincides with the network constant's maximum value (c=16.065). The degree of Crystallinity calculations further demonstrates that the best ratio (63.51%) was at a concentration (x = 0.05), confirming that is the optimum substitution ratio in comparison to the other substituents.

The (W-H) system only considers peak widening as a function of a diffraction angle (2θ), which is anticipated to have been a mix of

size-induced broadening and strain-induced broadening.

As opposed to this, the (SSP) approach, which analyzes peak profiles, simply takes into account the impact of crystalline size on XRD peak broadening and says nothing about the lattice microstructures. In the (HW) approach, peak broadening is thought to be a symmetrical Voigt function.

Acknowledgment:

We appreciate the cooperation of the Department of Physics at the College of Education for Girls at the University of Kufa and the cooperation of the superconducting laboratory official at the College of Education, Ibn Al-Haitham at the University of Baghdad.

5. REFERENCES

[1] A. Sacco, Electrochemical impedance spectroscopy: Fundamentals and application in dye-sensitized solar cells, Renewable and Sustainable Energy Reviews, 79 (2017) 814-829.

[2] Z. Alborzi, V. Daadmehr, Isovalent substitution effects of arsenic on structural and electrical properties of iron-based superconductor NdFeAsO0. 8F0. 2, Journal of Superconductivity and Novel Magnetism, 33 (2020) 387-396.

[3] M.R. Jobayr, S. Mahdi, E. Salman, K. Jasim, Effect of antimony on characteristics of HgBa 2 CaCu 2-x Sb x O 8+ δ superconducting, Journal of Ovonic Research, 18 (2022).

[4] H.M. Haider, K.M. Wadi, H.A. Mahdi, K.A. Jasim, A.H. Shaban, Studying the partial substitution of barium with cadmium oxide and its effect on the electrical and structural properties of HgBa2Ca2Cu3O8+ δ superconducting compound, in: AIP Conference Proceedings, AIP Publishing LLC, 2019, pp. 020033.

[5] M.K. Kamil, M.A. Hasan, K.A. Jasim, A.H. Shaban, Synthesis of HgSr2-xYxCa2Cu3O8+ δ Superconducting Compound, in: Key Engineering Materials, Trans Tech Publ, 2021, pp. 42-47.

[6] A. Arya, A. Sharma, Structural, electrical properties and dielectric relaxations in Na+-ion-conducting solid polymer electrolyte, Journal of Physics: Condensed Matter, 30 (2018) 165402.

[7] M.R. Jobayr, A.H.A. Al Razak, S.H. Mahdi, R.N. Fadhil, Study optoelectronic properties for polymer composite thick film, in: AIP Conference Proceedings, AIP Publishing LLC, 2018, pp. 030021.

[8] S.B. Ocak, A. Selçuk, S. Bayram, A. Ozbay, Frequency dependent dielectric properties of Al/maleic anhydride (MA)/p-Si structures, arXiv preprint arXiv:1604.07789, (2015).

[9] C. Chu, L. Deng, B. Lv, Hole-doped cuprate high temperature superconductors, Physica C: Superconductivity and its Applications, 514 (2015) 290-313.

[10] K.A. Jasim, L. Mohammed, The partial substitution of copper with nickel oxide on the Structural and electrical properties of HgBa2 Ca2 Cu3xNix O8+ δ superconducting compound, in: Journal of Physics: Conference Series, IOP Publishing, 2018, pp. 012071.

[11] L.A. Mohammed, K.A. Jasim, Improvement the Superconducting properties of TlBa2 Ca2 Cu3xNix O 9-δ superconducting compound by partial substitution of copper with

nickel oxide on the, Energy Procedia, 157 (2019) 135-142.

[12] F.B. Azzouz, A. M'chirgui, B. Yangui, C. Boulesteix, M.B. Salem, Synthesis, microstructural evolution and the role of substantial addition of PbO during the final processing of (Bi, Pb)-2223 superconductors, Physica C: Superconductivity, 356 (2001) 83-96.

[13] K. Jassim, Influence of Simultaneous Doping of Tl on the Transition Temperature Tc and the Lattice Parameters of HgBa2Ca2Cu3O8+ δ Superconductors, Ibn Al-Haitham Journal For Pure And Applied Science, 22 (2009).

[14] A. Shaban, L. Mohammed, H. Hussein, K. Jasim, The structural properties of Y 1-X La X Ba 4 Cu 7 O 15+ δ superconductor compound, Digest Journal of Nanomaterials & Biostructures (DJNB), 17 (2022).

[15] M.K. Kamil, K.A. Jasim, Calculating of crystalline size, strain and Degree of crystallinity of the compound (HgBa2Ca2Cu3O8+ σ) by different method, in: IOP Conference Series: Materials Science and Engineering, IOP Publishing, 2020, pp. 072109.

[16] H.P. Klug, L.E. Alexander, X-ray diffraction procedures: for polycrystalline and amorphous materials, 1974.

[17] D. Nath, F. Singh, R. Das, X-ray diffraction analysis by Williamson-Hall, Halder-Wagner and size-strain plot methods of CdSe nanoparticles-a comparative study, Materials Chemistry and Physics, 239 (2020) 122021.

[18] W. Hall, X-ray line broadening in metals, Proceedings of the Physical Society. Section A, 62 (1949) 741.

[19] V. Mote, Y. Purushotham, B. Dole, Williamson-Hall analysis in estimation of lattice strain in nanometer-sized ZnO particles, Journal of theoretical and applied physics, 6 (2012) 1-8.

[20] M. Barsoum, Fundamentals of ceramics, CRC press, 2019.

[21] B.S. Mitchell, An introduction to materials engineering and science for chemical and materials engineers, John Wiley & Sons, 2004.

[22] M.K. Kamil, K.A. Jasim, Investigation the Crystalline Size and Strain of Perovskite (YBa2Cu3O6) by variant method, Test Engineering and Management, 8719 (2020) 8719-8723.